JACS
JOURNAL OF THE AMERICAN CHEMICAL SOCIETY
Article
pubs.acs.org/JACS

Stabilization of a Ruthenium(II) Polypyridyl Dye on Nanocrystalline TiO_2 by an Electropolymerized Overlayer

Alexander M. Lapides,[†] Dennis L. Ashford,[†] Kenneth Hanson, Daniel A. Torelli, Joseph L. Templeton,* and Thomas J. Meyer*

Department of Chemistry, University of North Carolina at Chapel Hill, CB 3290, Chapel Hill, North Carolina 27599, United States

Supporting Information

ABSTRACT: The long-term performance of dye-sensitized solar and photoelectrochemical cells is strongly dependent on the stability of surface-bound chromophores and chromophore−catalyst assemblies at metal oxide interfaces. We report here electropolymerization as a strategy for increasing interfacial stability and as a simple synthetic route for preparing spatially controlled, multicomponent films at an interface. We demonstrate that $[Fe(v\text{-}tpy)_2]^{2+}$ (v-tpy = 4′-vinyl-2,2′:6′,2″-terpyridine) can be reductively electropolymerized on nanocrystalline TiO_2 functionalized with a phosphonate-derivatized Ru(II) polypyridyl chromophore. The outer:inner Fe:Ru ratio can be controlled by the number of reductive electrochemical scan cycles as shown by UV−visible absorption and energy dispersive X-ray spectroscopy measurements. Overlayer electropolymerization results in up to 30-fold enhancements in photostability compared to the surface-bound dye alone. Transient absorbance measurements have been used to demonstrate that photoexcitation and electron injection by the MLCT excited state(s) of the surface-bound Ru^{II} complex is followed by directional, outside-to-inside, $Fe^{II} \rightarrow Ru^{III}$ electron transfer. This strategy is appealing in opening a new approach for synthesizing surface-stabilized chromophore−catalyst assemblies on nanocrystalline metal oxide films.

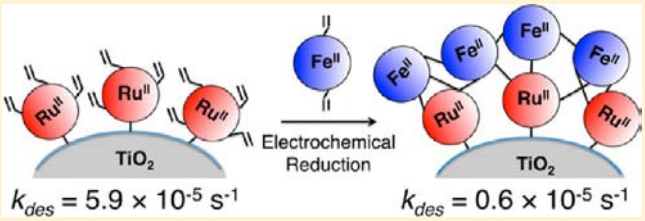

INTRODUCTION

Stable surface binding of chromophores, catalysts, and chromophore−catalyst assemblies on metal oxide surfaces is an essential element in dye-sensitized photoelectrochemical cells (DSPECs) for solar fuel production.[1−5] In a DSPEC for water oxidation, photoexcitation of a chromophore, or dye, followed by excited state electron injection into the conduction band of a high band gap semiconductor, typically TiO_2, provides the basis for a photoanode.[2] Oxidative equivalents produced by electron injection are subsequently transferred to a catalyst for water oxidation. The injected electrons are transferred to a cathode for reduction of either water to H_2 or CO_2 to carbon-containing fuels.[6,7] The design of water oxidation DSPEC photoanodes is particularly challenging because of the need to integrate both light absorption and catalysis at the oxide interface. The resulting interfacial structures must be stable under irradiation while supporting high numbers of turnovers in aqueous environments.[8,9]

A number of strategies for binding chromophores and catalysts to metal oxide surfaces have been reported. They include codeposition,[10,11] preformed assemblies,[12,13] and self-assembled bilayers.[14] These strategies are often limited by difficult synthetic procedures. The stability of the films, critical in all applications, is limited by the nature of the link to the surface. Although often used successfully in nonaqueous solvents, carboxylate−surface binding is unstable in water. Phosphonate−surface binding is far more robust but typically subject to hydrolysis from the surface at pH 5 and above.[8,9,15]

Oxidative or reductive electropolymerization provides a potentially useful strategy for preparing stable, multiple component films.[16−21] Reductive electropolymerization of vinyl-derivatized monomers is especially well developed.[22−29] In these reactions, electrochemical reduction of the vinyl-group induces radical polymerization and C−C coupling and bond formation.[23] On planar electrode surfaces, two or more redox carriers have been incorporated into spatially segregated copolymeric films by sequential reductive cycling in distinct monomer solutions, and into integrated copolymeric films prepared by cycling in a single solution containing multiple monomers.[22,24,30]

Despite the impressive background on planar electrodes, few reports have appeared describing electropolymerization on nanocrystalline metal oxide films.[26,27] In one notable example, Moss et al. demonstrated reductive electropolymerization of an overlayer of $[Ru(vbpy)_3]^{2+}$ (vbpy = 4-vinyl-4′-methyl-2,2′-bipyridine) on $[Ru(dcb)(vbpy)_2]^{2+}$ (dcb = 2,2′-bipyridine-4,4′-dicarboxylic acid) that had been prebound to nanocrystalline TiO_2. Significant increases in thermal stability for the surface-bound complex were observed even in basic media with no loss of chromophore over a three week period under conditions where the unprotected surface-bound complex underwent complete desorption in minutes.[26] The photostability and

Received: June 4, 2013
Published: September 2, 2013

   dx.doi.org/10.1021/ja4055977 | J. Am. Chem. Soc. 2013, 135, 15450−15458

photophysical properties of the resulting overlayer structures were relatively unexplored.[9]

The electropolymerized overlayer approach to surface assembly stabilization is promising. We report here the synthesis and characterization, including photostability and photophysical measurements, on multicomponent films on mesoporous TiO_2 prepared by reductive overlayer electropolymerization. The films were prepared by first derivatizing mesoporous TiO_2 with $[Ru(5,5'\text{-divinyl-}2,2'\text{-bipyridine})_2(4,4'\text{-}(PO_3H_2)_2\text{-bpy})]^{2+}$ (**RuPdvb** in Figure 1a, 4,4′-$(PO_3H_2)_2$-bpy = [2,2′-bipyridine]-4,4′-diylbis(phosphonic acid)) followed by reductive electropolymerization of [Fe(4′-vinyl-2,2′:6′:2″-terpyridine)$_2$]$^{2+}$ ([**Fe(v-tpy)$_2$**]$^{2+}$ in Figure 1a) to generate an electropolymerized overlayer. A scheme illustrating the formation of the TiO_2-**RuPdvb**-*poly*-[**Fe(v-tpy)$_2$**]$^{2+}$ overlayer structure is shown in Figure 1b.

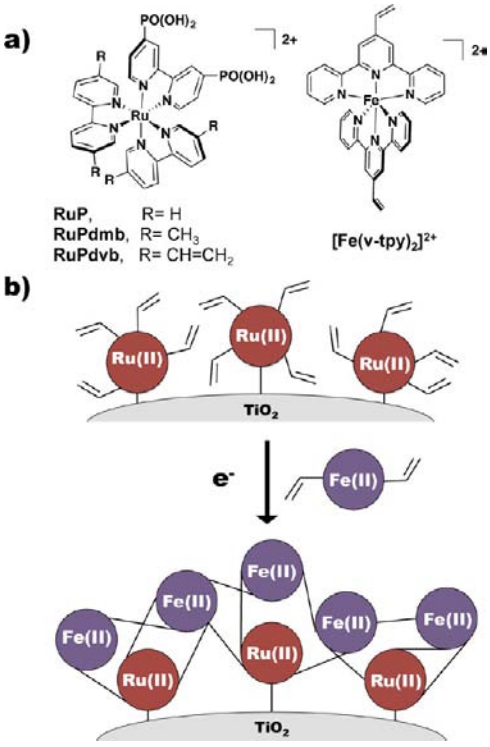

Figure 1. (a) Structures of **RuP**, **RuPdmb**, **RuPdvb** and [**Fe(v-tpy)$_2$**]$^{2+}$. (b) Schematic diagram of the surface structure following reductive polymerization of [**Fe(v-tpy)$_2$**]$^{2+}$ on TiO_2-**RuPdvb**.

RESULTS AND DISCUSSION

Monomer Synthesis and Characterization. The structures of the complexes investigated in this study are shown in Figure 1a. They were synthesized as chloride (Ru^{II} complexes) and hexafluorophosphate ([**Fe(v-tpy)$_2$**]$^{2+}$) salts. [**Fe(v-tpy)$_2$**]$^{2+}$ and **RuP** were synthesized by previously reported procedures.[25,31] **RuPdvb** and **RuPdmb** were synthesized by literature procedures with minor modification.[31] The starting complex, $Ru(5,5'\text{-}(R)_2\text{-bpy})_2Cl_2$ (R = CH_3 or $CH{=}CH_2$) was synthesized by heating $[Ru(1,4\text{-cyclooctadiene})Cl_2]_n$ and the bipyridine precursors in *o*-dichlorobenzene to 160 °C. The dichloride complexes were subsequently reacted with one equivalent of tetraethyl [2,2′-bipyridine]-4,4′-diylbis-(phosphonate) in a microwave reactor. The ethyl esters were then hydrolyzed using TMSBr in anhydrous acetonitrile to give the unprotected phosphonic acids. **RuPdvb** and **RuPdmb** were isolated as their chloride salts in 86% and 80% yield, respectively.

RuPdvb contains one phosphonated bipyridine ligand for binding to metal oxide surfaces and two bipyridine ligands with vinyl groups in the 5,5′ positions for electropolymerization. [**Fe(v-tpy)$_2$**]$^{2+}$ was selected as the monomer precursor for the polymer overlayer because of its readily discernible photophysical and electrochemical properties compared to **RuPdvb**. Following electropolymerization the vinyl groups of **RuPdvb** are converted by C−C coupling into saturated alkyl substituents.[23] Alkyl-substituted **RuPdmb** (R = CH_3 in Figure 1a) was used as a model for the surface bound chromophore following electropolymerization. **RuP** was used as the control chromophore for transient absorption and photostability experiments because its properties are well understood.[8,9]

In aqueous solutions, the absorption spectra for **RuP**, **RuPdvb** and **RuPdmb** all feature characteristic, intense $\pi-\pi^*$ absorptions below 350 nm and lower energy metal-to-ligand charge-transfer (MLCT) absorptions from 400 to 500 nm (Table 1, Figure S3 in the Supporting Information). The slight blue-shift in absorption for **RuPdvb** and red-shift in absorption for **RuPdmb** relative to **RuP** is due to stabilization/destabilization effects in the $d\pi^5\pi^*$ MLCT excited states by the electron-withdrawing vinyl and -donating methyl groups, respectively. [**Fe(v-tpy)$_2$**]$^{2+}$ has a MLCT absorption band maximum at 565 nm (ε = 15,500 M^{-1} cm^{-1}, Figure S3 in the Supporting Information).

Surface Loading. Adsorption isotherms were measured by immersing TiO_2 films (~7 μm thickness) in 10 mL solutions of 10, 20, 50, 100, 150, and 200 μM **RuP**, **RuPdvb**, and **RuPdmb** in methanol. Adsorption isotherms (Figure S4 in the Supporting Information) were analyzed by the Langmuir isotherm model.[32] Adsorption constants (K_{ad}) and maximum

Table 1. Photophysical, Electrochemical and Surface Binding Parameters for RuP, RuPdvb, RuPdmb and [Fe(v-tpy)$_2$]$^{2+}$ in Solution and on Metal Oxide Films

complex	MLCT λ_{max} (nm) (ε, M^{-1} cm^{-1})[a]	Γ_{max} (mol cm^{-2})	K_{ad} (M^{-1})	$E_{1/2}(Ru^{III/II})$ (V vs $Ag/AgNO_3$)[b]	$E_{1/2}(Ru^{III/II})$ (V vs NHE)[c]	ΔG_{ES} (eV)[d]	$E^{o\prime}$ ($Ru^{III/II*}$)[f] (V vs NHE)
RuP	458 (12,700)	8.5×10^{-8}	3.9×10^4	1.02	1.28	2.04	−0.76
RuPdvb	476 (13,300)	6.7×10^{-8}	2.2×10^4	1.12	1.34	2.02	−0.68
RuPdmb	453 (13,500)	5.2×10^{-8}	5.2×10^5	0.94	1.22	2.06	−0.84
[**Fe(v-tpy)$_2$**]$^{2+}$	565 (15,500)	–	–	0.79($Fe^{III/II}$)	–	*e*	–

[a]In H_2O. [b]In 0.1 M $TBAPF_6$ CH_3CN; planar FTO working, Pt counter, and $Ag/AgNO_3$ reference electrode (−0.09 V vs $Fc^{0/+}$). [c]In aqueous 0.1 M $HClO_4$, *nano*-TiO_2 working, Pt counter, and Ag/AgCl reference electrode (0.198 V vs NHE). [d]ΔG_{ES} from spectral fitting of emission on ZrO_2 in aqueous 0.1 M $HClO_4$ (Supporting Information). [e]Emission was not observed. [f]$E^{o\prime}(Ru^{III/II*}) = E_{1/2}(Ru^{III/II}) - \Delta G_{ES}$.

dx.doi.org/10.1021/ja4055977 | J. Am. Chem. Soc. 2013, 135, 15450−15458

surface coverages (Γ_{max}) were similar for all three complexes; the results are summarized in Table 1.

Surface Characterization. The electrochemical properties of **RuP**, **RuPdvb**, and **RuPdmb** on TiO_2 were examined by cyclic and square-wave voltammetry in CH_3CN (0.1 M $TBAPF_6$ electrolyte) and in aqueous 0.1 M $HClO_4$. The values are reported in Table 1. All complexes exhibit reversible $Ru^{III/II}$ couples with $E_{1/2}$ values of 1.28, 1.34, and 1.22 V (vs NHE in aqueous 0.1 M $HClO_4$) for **RuP**, **RuPdvb**, and **RuPdmb**, respectively (Figure S5 in the Supporting Information). Similar to the trends observed in absorption and emission spectra, the positive and negative shifts in $E_{1/2}$ for **RuPdvb** and **RuPdmb**, relative to **RuP**, can be attributed to the electron-withdrawing vinyl and electron-donating methyl groups, respectively.

Emission spectra for **RuP**, **RuPdvb**, and **RuPdmb** on ZrO_2 in aqueous 0.1 M $HClO_4$ were obtained (Figure S6 in the Supporting Information). The trends in emission parallel those observed for absorption. The emission spectra were analyzed by application of a one-mode Franck−Condon analysis with the procedure described elsewhere.[8,33,34] The free energy content of the thermally equilibrated ^{3}MLCT excited states (ΔG_{ES}) are given in Table 1 with the remaining spectral fitting parameters reported in Table S1 in the Supporting Information. Excited state reduction potentials for the couples, $Ru^{III} + e^- \rightarrow Ru^{II*}$ ($E^{\circ\prime}(Ru^{III/II*})$), were calculated from $E^{\circ\prime}(Ru^{III/II*}) = E_{1/2}(Ru^{III/II}) - \Delta G_{ES}$. Based on these values, all three complexes are sufficiently reducing (−0.68 to −0.84 V) to inject into the conduction band of TiO_2 (∼−0.5 V vs NHE) in aqueous pH 1 $HClO_4$.[35]

Polymerization of $[Fe(v\text{-}tpy)_2]^{2+}$ on FTO. It has previously been demonstrated that $[Fe(v\text{-}tpy)_2]^{2+}$ will undergo reductive electropolymerization on planar electrodes if the applied potential is more negative than the first v-tpy-based reduction potential (approximately −1.5 V vs $Ag/AgNO_3$).[25,36] As a control experiment, we initially investigated the electropolymerization of $[Fe(v\text{-}tpy)_2]^{2+}$ on a planar fluoride-doped tin oxide (FTO) slide. In these experiments FTO was used as the working electrode, platinum as the counter electrode and $Ag/AgNO_3$ as the reference electrode with $[Fe(v\text{-}tpy)_2]^{2+}$ in dry acetonitrile and 0.1 M $TBAPF_6$ as the electrolyte. The surface coverage (Γ in mol/cm^2) of redox active complex was calculated by using eq 1 where Q is the integrated current under the $Fe^{III/II}$ redox couple, F is Faraday's constant (96,485 C), n is the number of electrons transferred (n = 1), and A is the area of the electrode (∼1 cm^2).

$$\Gamma = Q/nFA \quad (1)$$

The applied potential was cycled from 0 to −1.8 V (vs $Ag/AgNO_3$), and FTO surface coverage was monitored as a function of both scan rate (50, 100, and 200 mV s^{-1}) and $[Fe(v\text{-}tpy)_2]^{2+}$ concentration (0.5, 1.0, and 2.0 mM). Surface coverage was found to increase linearly as scan rate decreased or as the $[Fe(v\text{-}tpy)_2]^{2+}$ concentration was increased (Figure S7 in the Supporting Information).

Polymerization of $[Fe(v\text{-}tpy)_2]^{2+}$ on *nano*-TiO_2. Under sufficiently reducing potentials (more negative than −0.5 V vs NHE at pH = 1)[35] nanocrystalline TiO_2 can readily transport electrons from the FTO electrode, through the metal oxide film, to the TiO_2−electrolyte interface providing a basis for reductive electropolymerization of $[Fe(v\text{-}tpy)_2]^{2+}$. The high effective surface area of *nano*-TiO_2 allows for monitoring the surface coverage of *poly*-$[Fe(v\text{-}tpy)_2]^{2+}$ ($\varepsilon_{565\ nm}$ = 15,500 M^{-1} cm^{-1}) by UV/visible absorption measurements. Absorption changes during an electropolymerization on a TiO_2 film cycled from 0 to −1.8 V vs $Ag/AgNO_3$ are shown in Figure 2.

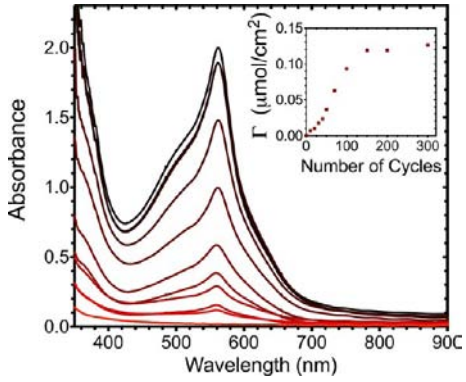

Figure 2. Changes in UV/visible absorption spectra for TiO_2 (dry slide) as the number of reductive cycles from 0 to −1.8 V (vs $Ag/AgNO_3$) is increased (0, 10, 20, 30, 40, 50, 70, 100, 150, 200 and 300; red to black) in an acetonitrile solution of 0.5 mM $[Fe(v\text{-}tpy)_2]^{2+}$ (0.1 M $TBAPF_6$ electrolyte); Pt counter electrode, and $Ag/AgNO_3$ reference electrode. Inset: Surface coverage of *poly*-$[Fe(v\text{-}tpy)_2]^{2+}$ versus the number of reductive cycles.

For the first 70 cycles the surface coverage of *poly*-$[Fe(v\text{-}tpy)_2]^{2+}$ increases linearly with the number of cycles (inset, Figure 2) and continues to increase, albeit at a slower rate, from 70 to 150 cycles. Further polymerization was minimal after 150 cycles. At 70 cycles, a single monolayer of *poly*-$[Fe(v\text{-}tpy)_2]^{2+}$ was deposited on the TiO_2 surface (∼7 × 10^{-8} mol cm^{-2}) as determined by UV/visible absorption measurements. The decreased deposition rate for $[Fe(v\text{-}tpy)_2]^{2+}$ from 70 to 150 cycles may be due to a decrease in the rate of electron transfer from TiO_2 to $[Fe(v\text{-}tpy)_2]^{2+}$ or a decrease in the available volume within the internal voids of the nanostructured films. In any case, electropolymerization is hindered after the deposition of approximately two monolayers (150 cycles), Figure 2, inset.

No change in absorption was observed for a TiO_2 electrode cycled in $[Fe(v\text{-}tpy)_2]^{2+}$ solution from 0 V to −1.0 V (vs $Ag/AgNO_3$). This potential range is more positive than that required for reductive electropolymerization, and this result shows that physical adsorption of $[Fe(v\text{-}tpy)_2]^{2+}$ to TiO_2 prior to electropolymerization does not occur.

Polymerization of $[Fe(v\text{-}tpy)_2]^{2+}$ on *nano*-TiO_2-RuPdvb. Electropolymerized films of TiO_2-**RuPdvb**-*poly*-$[Fe(v\text{-}tpy)_2]^{2+}$ were prepared by first derivatizing TiO_2 with a monolayer of **RuPdvb** (TiO_2-**RuPdvb**) by loading from methanol. The TiO_2-**RuPdvb** film was then used as the working electrode during reductive cycling in an acetonitrile solution of 0.5 mM $[Fe(v\text{-}tpy)_2]^{2+}$ (0.1 M $TBAPF_6$ electrolyte). The changes in the UV/visible absorption spectra of TiO_2-**RuPdvb** with increasing number of reductive cycles from 0 to −1.8 V (vs $Ag/AgNO_3$) is shown in Figure 3.

UV/visible absorption spectra of the polymerized films showed that the MLCT band for **RuPdvb** did not diminish in intensity following reductive polymerization of $[Fe(v\text{-}tpy)_2]^{2+}$ (Figure 3a). As with nonderivatized TiO_2 (see above) the surface coverage of *poly*-$[Fe(v\text{-}tpy)_2]^{2+}$ increases approximately linearly from 0 to 70 cycles, slows from 70 to 150 cycles, then remains constant above 150 cycles (Figure 3b). The surface coverage of *poly*-$[Fe(v\text{-}tpy)_2]^{2+}$ on TiO_2-**RuPdvb** after 70 and 150 cycles corresponds to approximately one and two monolayers, respectively.

dx.doi.org/10.1021/ja4055977 | J. Am. Chem. Soc. 2013, 135, 15450−15458

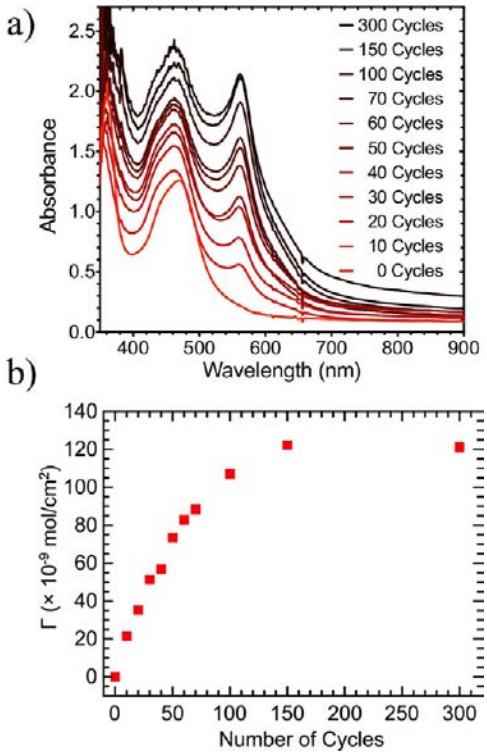

Figure 3. (a) Changes in UV/visible absorption spectra for TiO_2-**RuPdvb** (dry slide) with an increase in the number of reductive scan cycles from 0 to −1.8 V (vs $Ag/AgNO_3$) in an acetonitrile solution 0.5 mM in $[\mathbf{Fe(v\text{-}tpy)_2}]^{2+}$ (0.1 M $TBAPF_6$ electrolyte); Pt counter electrode, and $Ag/AgNO_3$ reference electrode. (b) Surface coverage of *poly*-$[\mathbf{Fe(v\text{-}tpy)_2}]^{2+}$ versus the number of scan cycles.

A blue-shift (~9 nm) in the MLCT band for **RuPdvb** was observed after the first 10 cycles of electropolymerization (Figure 3a). A similar blue-shift (Figure S8 in the Supporting Information) is also observed for TiO_2-**RuPdvb** after reductive cycling in 0.5 mM *p*-divinylbenezene (absorption <350 nm) showing that the shift in Ru^{II}-based absorption in TiO_2-**RuPdvb**-*poly*-$[\mathbf{Fe(v\text{-}tpy)_2}]^{2+}$ is not due to $[\mathbf{Fe(v\text{-}tpy)_2}]^{2+}$. The absorption spectrum of TiO_2-**RuPdvb** after electropolymerization closely resembles that of TiO_2-**RuPdmb**, suggesting that the shift is due to conversion of the electron-withdrawing vinyl groups in **RuPdvb** to saturated alkane groups formed during the polymerization process.[23]

The electrochemical properties of TiO_2-**RuPdvb** were monitored before and after reductive polymerization by cyclic voltammetry. Oxidative scans from 0 to 1.5 V (vs $Ag/AgNO_3$) in CH_3CN (0.1 M $TBAPF_6$) following successive reductive cycles from 0 to −1.8 V (vs $Ag/AgNO_3$) are shown in Figure 4. TiO_2 is a wide band gap semiconductor with $E_{vb} \approx 2.8$ V at pH = 7, and Ru^{II} oxidation to Ru^{III} on the surface is initiated by electron transfer at the FTO interface followed by cross-TiO_2 surface Ru(II) → Ru(III) electron transfer hopping with associated counterion diffusion.[35,37]

Before overlayer electrodeposition, $E_{1/2}(Ru^{III/II})$ appeared at 1.16 V (vs $Ag/AgNO_3$). Upon electropolymerization of the overlayer, the peak current for the $Ru^{III/II}$ couple decreased and the peak-to-peak splitting increased. Past ~50 cycles from 0 to 1.5 V (vs $Ag/AgNO_3$) at 50 mV/s, the couple is no longer observed. Nonetheless, after 50 cycles the MLCT absorption band for **RuPdvb** is relatively unchanged in UV/vis absorption spectra (Figure 3a), indicating that it is still on the surface. A

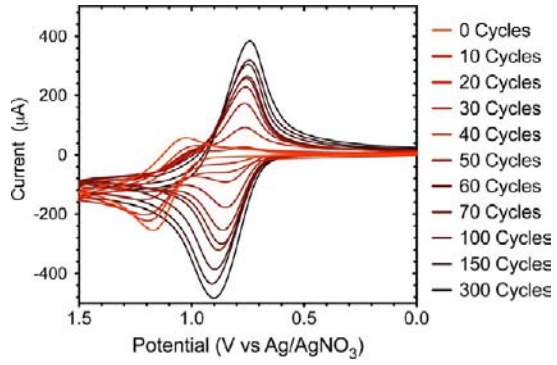

Figure 4. Cyclic voltammograms for TiO_2-**RuPdvb** from 0 to 1.5 V (vs $Ag/AgNO_3$) in CH_3CN (0.1 M $TBAPF_6$) after successive reductive scan cycles (100 mV/s) in CH_3CN solution 0.5 mM in $[\mathbf{Fe(v\text{-}tpy)_2}]^{2+}$, 0.1 M in $TBAPF_6$; Pt counter electrode; $Ag/AgNO_3$ reference electrode.

likely explanation for the decrease and ultimate loss in current for the $Ru^{III/II}$ wave is a blocking effect by the growing *poly*-$[\mathbf{Fe(v\text{-}tpy)_2}]^{2+}$ overlayer film which inhibits diffusion of counterions to the Ru^{II} sites on the surface. The lack of counterion diffusion, and thus charge balance, for oxidation of Ru^{II} to Ru^{III} potentially inhibits cross-surface electron transfer.

After polymerization, a new reversible $Fe^{III/II}$ couple, due to *poly*-$[\mathbf{Fe(v\text{-}tpy)_2}]^{2+}$, is observed at $E_{1/2}$ = 0.85 V (vs $Ag/AgNO_3$). The integrated current for the $Fe^{III/II}$ wave increases with each successive reductive cycle.

Morphology Characterization. The morphology and composition of the TiO_2-**RuPdvb**-*poly*-$[\mathbf{Fe(v\text{-}tpy)_2}]^{2+}$ films were examined by scanning electron microscopy (SEM) and energy-dispersive X-ray spectroscopy (EDS). SEM images of TiO_2-**RuPdvb** following 50 and 300 cycles of reductive polymerization can be seen in Figure 5. The SEM image of TiO_2-**RuPdvb**-*poly*-$[\mathbf{Fe(v\text{-}tpy)_2}]^{2+}$ after 50 reductive cycles resembles that of TiO_2-**RuPdvb** in that the porosity of the nanocrystalline TiO_2 is retained after polymerization (Figures 5a and 5c). In contrast, after 300 reductive cycles, the porosity of the film is reduced and a film of *poly*-$[\mathbf{Fe(v\text{-}tpy)_2}]^{2+}$ has formed on top of the mesoporous TiO_2 film (Figures 5b and 5d). Presumably, as noted above, the surface layer inhibits both substrate and electrolyte diffusion into the film, with the latter resulting in the decrease in current for the $Ru^{III/II}$ couple.

EDS was used to determine the concentrations of ruthenium and iron at different depths within the TiO_2 films. The results are summarized in Table 2. The EDS data for TiO_2-**RuPdvb**-*poly*-$[\mathbf{Fe(v\text{-}tpy)_2}]^{2+}$ films prepared from 50 and 300 reductive cycles both reveal inhomogeneities throughout the mesoporous structure and a gradient in ruthenium complex content as well. The concentration of surface-bound Ru^{II} complex is highest at the TiO_2−solution interface (top, Figures S1 and S2 in the Supporting Information) decreasing with depth toward the FTO surface (bottom, Figures S1 and S2 in the Supporting Information). This result is consistent with those of O'Regan et al., which demonstrated that standard dye loading procedures on TiO_2 do not uniformly coat the films, but instead result in greater dye loading near the surface.[38]

The EDS results also show that the Fe:Ru ratio is higher at the TiO_2−solution interface (top) compared to the interior of the film. This result suggests that electropolymerization of $[\mathbf{Fe(v\text{-}tpy)_2}]^{2+}$ occurs rapidly at the TiO_2−solution interface but is limited by diffusion of $[\mathbf{Fe(v\text{-}tpy)_2}]^{2+}$ into the

dx.doi.org/10.1021/ja4055977 | J. Am. Chem. Soc. 2013, 135, 15450−15458

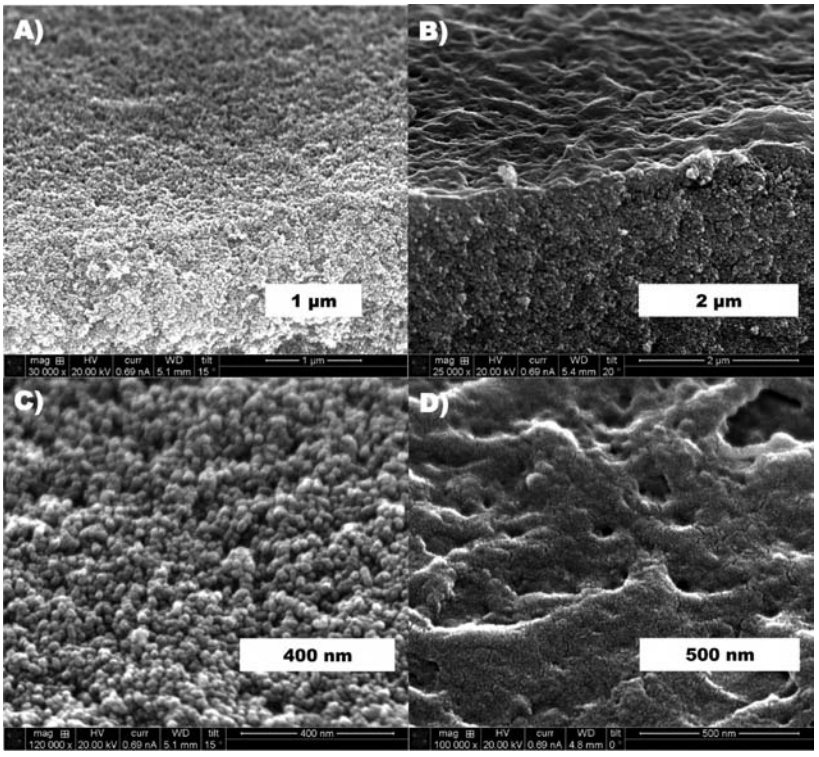

Figure 5. Cross-sectional (A and B) and surface (C and D) SEM images of the TiO_2-**RuPdvb** film following 50 (A and C) and 300 (B and D) reductive cycles in an CH_3CN solution containing 0.5 mM $[\mathbf{Fe(v\text{-}tpy)_2}]^{2+}$.

Table 2. The Atomic % and Ru:Fe Ratios at the Top, Middle and Bottom of TiO_2-RuPdvb Films after 50 and 300 Reductive Cycles (100 mV/s) in an Acetonitrile Solution Containing 0.5 mM $[\mathbf{Fe(v\text{-}tpy)_2}]^{2+}$ (0.1 M $TBAPF_6$ Electrolyte)

sample	Ru atomic %	Fe atomic %	Ru:Fe
50 cycles-top	1.54	1.05	1:0.7
50 cycles-middle	1.31	0.62	1:0.5
50 cycles-bottom	0.88	0.43	1:0.5
300 cycles-top	0.50	1.20	1:2.4
300 cycles-middle	0.51	0.75	1:1.5
300 cycles-bottom	0.43	0.60	1:1.4

mesoporous TiO_2 network. As a result the Fe:Ru ratios determined by UV/visible absorption measurements represent averages of actual ratios throughout the inhomogeneously loaded films. The Ru:Fe ratios in TiO_2-**RuPdvb**-*poly*-$[\mathbf{Fe(v\text{-}tpy)_2}]^{2+}$ after 50 and 300 cycles, as determined by UV/visible absorption measurements, were 1:1 and 1:1.7, respectively. A film with a more uniform ratio of Fe:Ru was prepared by soaking a TiO_2-**RuPdvb** slide in a $[\mathbf{Fe(v\text{-}tpy)_2}]^{2+}$ solution (0.5 mM in 0.1 M $TBAPF_6/CH_3CN$) overnight, stirring the solution during the electropolymerization process, and pausing 60 s between each electropolymerization cycle (Figure S9 in the Supporting Information). This suggests that diffusion of $[\mathbf{Fe(v\text{-}tpy)_2}]^{2+}$ through the mesoporous TiO_2 is a significant factor when controlling the distribution of the ratio of bound dye to electropolymer overlayer in the formation of these films.

Photostability. The photostabilities of TiO_2-**RuPdvb**-*poly*-$[\mathbf{Fe(v\text{-}tpy)_2}]^{2+}$ relative to **RuP** and **RuPdvb** on TiO_2 were evaluated by a previously published procedure with constant irradiation at 455 nm (fwhm ~30 nm, 475 mW/cm^2, ~135 suns at 455 nm).[8,9] Absorption spectra (360−800 nm) of the films were obtained every 15 min during 16 h of irradiation. Results for TiO_2-**RuPdvb** with ~2 monolayers of *poly*-$[\mathbf{Fe(v\text{-}tpy)_2}]^{2+}$ (150 cycles) in aqueous 0.1 M $HClO_4$ (pH 1) are shown in Figure 6. The time-dependent changes in absorption

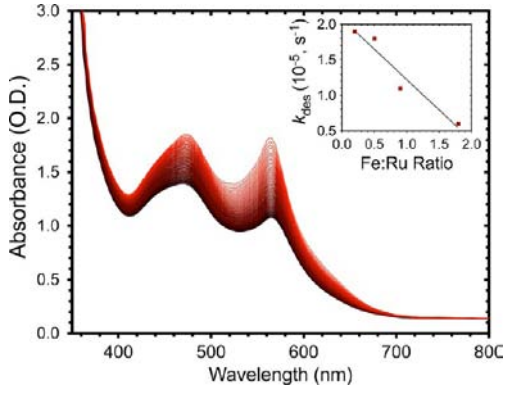

Figure 6. Changes in the absorption spectrum of TiO_2-**RuPdvb**-*poly*-$[\mathbf{Fe(v\text{-}tpy)_2}]^{2+}$ (150 cycles, 1:1.8 Ru:Fe) in aqueous 0.1 M $HClO_4$ under constant 455 nm irradiation (475 mW/cm^2) from 0 (red) to 16 h (black) recorded every 15 min. Inset: Desorption rate constant (k_{des}) as a function of the number of reductive cycles.

at 480 nm were fit with the biexponential function in eq S4 in the Supporting Information and are presented as a single average rate constant (k_{des}) calculated as the inverse of the weighted average lifetime ($k_{des} = \langle\tau\rangle^{-1}$) for the time-dependent absorption changes, eq S5 in the Supporting Information. The results are summarized in Tables 3 and 4.

Desorption rate constants for the unprotected surface-bound chromophores increase slightly in the order **RuP** (4.8×10^{-5} s^{-1}), **RuPdvb** (5.6×10^{-5} s^{-1}), and **RuPdmb** (5.8×10^{-5} s^{-1}).

dx.doi.org/10.1021/ja4055977 | J. Am. Chem. Soc. 2013, 135, 15450−15458

Table 3. Summary of Desorption Rate Constants (k_{des}) in Aqueous 0.1 M $HClO_4$ for RuP, RuPdvb, and RuPdmb on TiO_2 and TiO_2-RuPdvb Films after 10, 30, 70, and 150 Reductive Cycles in $[Fe(v\text{-}tpy)_2]^{2+}$ Solution

sample	Ru:Fe	k_{des} ($\times 10^{-5}$ s^{-1})
RuP	1:0	4.8
RuPdmb	1:0	5.6
RuPdvb	1:0	5.9
RuPdvb + 10 cycles	1:0.2	1.9
RuPdvb + 30 cycles	1:0.5	1.8
RuPdvb + 70 cycles	1:0.9	1.1
RuPdvb + 150 cycles	1:1.8	0.6

Table 4. Summary of Desorption Rate Constants (k_{des}) for TiO_2-RuP, TiO_2-RuP Stabilized by ~3.3 Å of Al_2O_3, and in TiO_2-RuPdvb-*poly*-$[Fe(v\text{-}tpy)_2]^{2+}$ Films (150 cycles, 1:1.8 Ru:Fe) under Various Conditions

	k_{des} ($\times 10^{-5}$ s^{-1})		
solvent	TiO_2-**RuP**	TiO_2-**RuP** + ~3.3 Å of Al_2O_3[e]	TiO_2-**RuPdvb**-*poly*-$[Fe(v\text{-}tpy)_2]^{2+}$
pH 1[a]	4.8	–	0.6
pH 5[b]	>20	2.3	1.3
H_2O	>30	3.2	0.9
pH 7[c]	–	9.5	5.5
CH_3CN[d]	0.8	<0.01	0.07

[a]0.1 M $HClO_4$. [b]10 μM $HClO_4$. [c]0.1 M Na_3PO_4 buffer. [d]0.1 M $LiClO_4$. [e]From ref 41.

All three complexes share a similar surface binding motif based on the 4,4′-$(PO_3H_2)_2$bpy) ligand, and the slight differences in k_{des} are presumably due to the differences in surface packing and morphology/local structure.

The photochemical desorption rate constants for TiO_2-**RuPdvb** in aqueous 0.1 M $HClO_4$ as a function of Ru:Fe ratios are summarized in Table 3 (Figure S10 in the Supporting Information). With 10 reductive cycles, 1:0.2 (Ru:Fe), k_{des} is three times slower than for unprotected TiO_2-**RuPdmb** or **RuPdvb**. From 10 (1:0.2 Ru:Fe) to 150 cycles, 1:1.8 (Ru:Fe), there was an approximately linear decrease in k_{des} from 4.8 $\times$ 10^{-5} s^{-1} to 0.6 $\times$ 10^{-5} s^{-1} (inset Figure 6). The desorption rate constant was similar from 400 to 600 nm, showing that desorption from the surface, and not photodecomposition of **RuPdvb** or $[Fe(v\text{-}tpy)_2]^{2+}$, is occurring.

The mechanism of photoinduced chromophore desorption from the metal oxide surface is not fully understood, but mechanisms have been proposed.[9] Increased stability after polymerization may arise from a number of factors including (1) increased steric bulk provided by the polymer, which inhibits hydroxide/water attack at the phosphonate groups on the surface; (2) cross-linking of the film, which mechanically prevents desorption of individual chromophores; and (3) the newly formed hydrophobic alkyl linkers, which reduce the solubility of the film in the external aqueous medium. Similar factors have been suggested for dye-sensitized solar cells that have been stabilized by cross-linking polymerization.[39]

It is also important to note that under irradiation a photostationary state exists that is dictated by photoexcitation, electron injection, and back electron transfer rates. For **RuP**, **RuPdvb**, and **RuPdmb** on TiO_2 under irradiation the surface-bound complex exists as Ru^{III}.[40] Conversely for TiO_2-**RuPdvb**-*poly*-$[Fe(v\text{-}tpy)_2]^{2+}$ there is a ~300 mV driving force for electron transfer from *poly*-$[Fe(v\text{-}tpy)_2]^{2+}$ to Ru^{III}**Pdvb**, and at the steady state Fe^{III} dominates (see below).

The desorption rate constant for the TiO_2-**RuPdvb**-*poly*-$[Fe(v\text{-}tpy)_2]^{2+}$ films (150 cycles, 1:1.8 Ru:Fe) was investigated in a variety of solvents, and the results are summarized in Table 4 (Figure S11 in the Supporting Information). In previous experiments, the photostability of TiO_2-**RuP** was maximized in 0.1 M $HClO_4$ with k_{des} (5.0 $\times$ 10^{-5} s^{-1}) increasing at higher pHs and in buffered solutions.[9] It is notable that at pH 5 (1.3 $\times$ 10^{-5} s^{-1}) and in H_2O (0.9 $\times$ 10^{-5} s^{-1}) the desorption rate constant for TiO_2-**RuPdvb**-*poly*-$[Fe(v\text{-}tpy)_2]^{2+}$ is lower than for TiO_2-**RuP** at pH 1 in water. Even in solutions buffered at pH 7 (0.1 M Na_3PO_4 buffer), the polymerized films have desorption rate constants (5.5 $\times$ 10^{-5} s^{-1}) comparable to TiO_2-**RuP** in 0.1 M $HClO_4$. In solutions buffered at pH 7, desorption of **RuP** occurs with k_{des} > 30 $\times$ 10^{-5} s^{-1}.

The use of the standard stability measurement protocol allows for comparison between surface stabilization strategies. For example, we recently demonstrated that atomic layer deposition (ALD) of Al_2O_3 on a TiO_2 surface derivatized with **RuP** significantly increases the stability of the surface-bound complex in water.[41] A comparison of k_{des} for untreated TiO_2-**RuP**, TiO_2-**RuP** stabilized by ~3.3 Å of ALD Al_2O_3, and TiO_2-**RuPdvb**-*poly*-$[Fe(v\text{-}tpy)_2]^{2+}$ films (150 cycles, 1:1.8 Ru:Fe) is shown in Table 4. Under aqueous conditions the polymerized films are almost twice as stable as the ALD films and 10 times more stable than the untreated films. This result suggests that reductive electropolymerization is a viable strategy for increasing stability of surface-bound complexes under aqueous conditions.

Transient Absorption. Interfacial electron transfer dynamics for TiO_2-**RuP**, TiO_2-*poly*-$[Fe(v\text{-}tpy)_2]^{2+}$, and TiO_2-**RuPdvb** with 10, 30, 70, and 150 cycles of *poly*-$[Fe(v\text{-}tpy)_2]^{2+}$ overlayer were investigated by nanosecond transient absorption measurements in aqueous 0.1 M $HClO_4$. It has previously been demonstrated that photoexcitation of phosphonate-derivatized ruthenium polypyridyl complexes on TiO_2, eq 2, is followed by efficient electron injection into the conduction band of TiO_2, eq 3, with Φ_{inj} = 100% for TiO_2-**RuP** at pH 1.[8] The electron injection process is accompanied by a bleach of the MLCT absorption features from 400 to 520 nm.

For TiO_2-*poly*-$[Fe(v\text{-}tpy)_2]^{2+}$ (70 cycles, ~1 monolayer), a negligible transient absorption response (<10 mOD at 580 nm) was observed upon photoexcitation at 450 nm (Figure S12 in the Supporting Information). The relatively small transient absorption amplitude suggests that the injection yield for excited *poly*-$[Fe(v\text{-}tpy)_2]^{2+}$ on TiO_2 is <1%, consistent with the known photophysics of related complexes in solution. As shown by McCusker, MLCT excitation is followed by rapid interconversion to low-lying dd states and rapid nonradiative decay.[42]

$$TiO_2\text{-}\mathbf{Ru^{II}} + h\nu \rightarrow TiO_2\text{-}\mathbf{Ru^{II}}* \quad (2)$$

$$TiO_2\text{-}\mathbf{Ru^{II}}* \rightarrow TiO_2(e^-)\text{-}\mathbf{Ru^{III}} \quad (3)$$

Time-resolved absorption difference spectra for **RuPdvb** with 10, 30, 70, and 150 cycles of *poly*-$[Fe(v\text{-}tpy)_2]^{2+}$ following photoexcitation at 425 nm were constructed from multiple single-wavelength measurements from 440 to 640 nm, acquired every 10 nm. The results are shown in Figure 7 and Figure S13 in the Supporting Information.

In the difference spectra for TiO_2-**RuPdvb**-*poly*-$[Fe(v\text{-}tpy)_2]^{2+}$ (1:0.5 Ru:Fe) in Figure 7, there is evidence for

dx.doi.org/10.1021/ja4055977 | J. Am. Chem. Soc. 2013, 135, 15450−15458

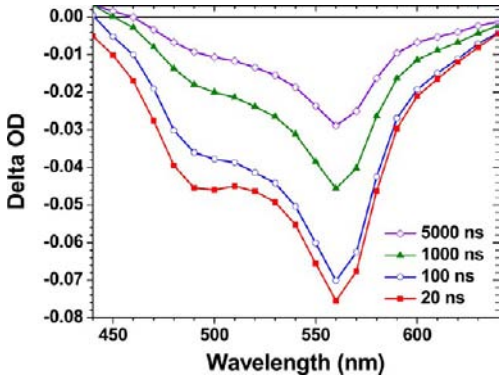

Figure 7. Time-resolved absorption difference spectra for TiO_2-**RuPdvb**-*poly*-[**Fe(v-tpy)$_2$**]$^{2+}$ (30 cycles, 1:0.5 Ru:Fe) in Ar deaerated aqueous 0.1 M $HClO_4$. (Excitation at 425 nm, 5.0 mJ/pulse).

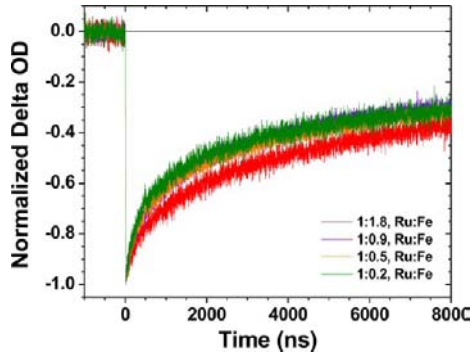

Figure 8. Absorption−time traces for TiO_2-**RuPdvb**-*poly*-[**Fe(v-tpy)$_2$**]$^{2+}$ with various ratios of Ru to Fe in Ar deaerated 0.1 M $HClO_4$ aqueous solutions monitored at 580 nm (450 nm excitation, 5.0 mJ/pulse).

electron injection because there is a loss in the MLCT absorbance for Ru^{II} from 450 to 520 nm and Fe^{II} from 520 to 640 nm. Following the laser flash, the bleach feature for Ru^{II} decreases more rapidly than the bleach feature for Fe^{II}.

The time-dependent absorption changes appear to arise from competing electron transfer events following photoexcitation (eq 4) and quenching of TiO_2-$\mathbf{Ru^{II}}$* (eq 5). They include back electron transfer from $TiO_2(e^-)$ to Ru^{III} (eq 6), interassembly/interlayer electron transfer from Fe^{II} to Ru^{III} (eq 7), and back electron transfer from $TiO_2(e^-)$ to Fe^{III} (eq 8). In these reactions, **RuPdvb** and *poly*-[**Fe(v-tpy)$_2$**]$^{2+}$ are represented by $\mathbf{Ru^{II}}$ and $\mathbf{Fe^{II}}$, respectively, and injection by $\mathbf{Fe^{II}}$* is neglected because it is negligible (Figure S12 in the Supporting Information).

$$TiO_2\text{-}\mathbf{Ru^{II}}\text{-}\mathbf{Fe^{II}} + h\nu \rightarrow TiO_2\text{-}\mathbf{Ru^{II}}^*\text{-}\mathbf{Fe^{III}} \quad (4)$$

$$TiO_2\text{-}\mathbf{Ru^{II}}^*\text{-}\mathbf{Fe^{II}} \rightarrow TiO_2(e^-)\text{-}\mathbf{Ru^{III}}\text{-}\mathbf{Fe^{II}} \quad (5)$$

$$TiO_2(e^-)\text{-}\mathbf{Ru^{III}}\text{-}\mathbf{Fe^{II}} \rightarrow TiO_2\text{-}\mathbf{Ru^{II}}\text{-}\mathbf{Fe^{II}} \quad (6)$$

$$TiO_2(e^-)\text{-}\mathbf{Ru^{III}}\text{-}\mathbf{Fe^{II}} \rightarrow TiO_2(e^-)\text{-}\mathbf{Ru^{II}}\text{-}\mathbf{Fe^{III}} \quad (7)$$

$$TiO_2(e^-)\text{-}\mathbf{Ru^{II}}\text{-}\mathbf{Fe^{III}} \rightarrow TiO_2\text{-}\mathbf{Ru^{II}}\text{-}\mathbf{Fe^{II}} \quad (8)$$

The spectral changes over time suggest that electron transfer from $\mathbf{Fe^{II}}$ to $\mathbf{Ru^{III}}$ (eq 7) occurs on a time scale of hundreds of nanoseconds. Quantitation is difficult in part because, as noted above, the TiO_2-**RuPdvb**-*poly*-[**Fe(v-tpy)$_2$**]$^{2+}$ overlayer structures are inhomogenous in composition with depth in the film. Transient absorption spectral changes include electron transfer events between localized regions with different Ru^{II}:Fe^{II} ratios. There is also kinetic overlap between intra-assembly $Fe^{II} \rightarrow Ru^{III}$ electron transfer (eq 7) and back electron transfer from $TiO_2(e^-)$ to Ru^{III} (eq 6) and Fe^{III} (eq 8). For **RuP** on TiO_2 back electron transfer extends from the nanosecond to millisecond time scales,[8] and as found for other dynamic processes at nanocrystalline metal oxide interfaces, the kinetics are nonexponential and highly complex.[43,44]

The spectral changes for oxidation/reduction of *poly*-[**Fe(v-tpy)$_2$**]$^{2+}$ can be differentiated from those arising from $Ru^{III/II}$ by measuring the relative electron injection yield and back electron transfer dynamics at 580 nm. This wavelength is the ground state/oxidized state isosbestic point for **RuPdmb**, the optical model for **RuPdvb** after polymerization. Absorption−time kinetic traces at 580 nm following 450 nm excitation are shown in Figure 8. The data were fit over the first ∼10 μs using the triexponential function in eq S1 in the Supporting Information. Weighted average lifetime values, ⟨τ⟩, calculated by use of eq S2 in the Supporting Information, are summarized in Table 5.

Table 5. Net Electron Injection Yields (Based on the Appearance of Fe^{III}), Average Back Electron Transfer Lifetimes, and k_{bet} from Transient Absorption Measurements on TiO_2-RuPdvb-*poly*-[Fe(v-tpy)$_2$]$^{2+}$ as a Function of Ru:Fe Ratio in 0.1 M $HClO_4$ with TiO_2-RuP as a Reference[a]

		lifetime (μs)				
Ru:Fe	Φ_{inj}[b]	t_1 (A_1)	t_2 (A_2)	t_3 (A_3)	⟨τ⟩	k_{bet} ($\times 10^4$ s^{-1})
1:0.2	0.15	0.20(1)	1.6(6)	16.5(94)	16.4	6.1
1:0.5	0.35	0.25(1)	1.8(4)	18.5(96)	18.4	5.4
1:0.9	0.30	0.23(1)	1.6(5)	18.2(95)	18.1	5.5
1:1.8	0.20	0.23(1)	1.6 (5)	21.3(95)	21.2	4.7
RuP[c]	1.00	0.01(2)	0.8(9)	10.7(89)	10.6	9.4

[a]Excitation at 450 nm, probed at 580 nm. [b]Δε for **Fe** at 580 nm is −11,200, for **RuP** at 400 nm is −6500. [c]Monitored at 400 nm.

In Figure 8, a bleach feature is present at 580 nm at the earliest observation of ∼20 ns. Given the lack of direct injection by Fe^{II}*, this feature is a marker for Ru^{II}* injection (eq 5) followed by partial intra-assembly $Fe^{II} \rightarrow Ru^{III}$ electron transfer. Based on these data there is a rapid electron transfer component occurring in less than 20 ns (eq 7). The bleach feature for Ru^{II}, Figure 7, is still present at >20 ns, which shows that another fraction of Ru^{III} sites produced by electron injection undergo relatively slow $Fe^{II} \rightarrow Ru^{III}$ (eq 7) electron transfer or return to Ru^{II} by back electron transfer from $TiO_2(e^-)$, eq 6.

Return of the bleach to the baseline by $TiO_2(e^-) \rightarrow Fe^{III}$ back electron transfer, eq 8, is ∼60% complete by 9 μs. As can be seen in Figure 8 and Table 5, there is a slight trend toward slower back electron transfer as the Ru:Fe ratio is increased from 1:0.2 ($k_{bet} = 6.1 \times 10^4$ s^{-1}) to 1:1.8 ($k_{bet} = 4.7 \times 10^4$ s^{-1}).

Relative electron injection efficiencies (Φ_{inj}) for TiO_2-**RuPdvb**-*poly*-[**Fe(v-tpy)$_2$**]$^{2+}$ were estimated by using thin film actinometry with TiO_2-**RuP** ($\Phi_{inj} = 1.0$) as the reference.[8,45] Amplitude changes were evaluated 10 ns following 450 nm laser excitation with injection yields calculated by using eq S3 in the Supporting Information from the experimental section with $\Delta\varepsilon = -6500$ M^{-1} cm^{-1} at 400 nm for **RuP** and $\Delta\varepsilon = -11{,}200$ M^{-1} cm^{-1} at 580 nm for *poly*-[**Fe(v-tpy)$_2$**]$^{2+}$. The latter were

dx.doi.org/10.1021/ja4055977 | J. Am. Chem. Soc. 2013, 135, 15450−15458

determined by spectroelectrochemical measurements on *nano*-ITO (Figure S14 in the Supporting Information). The results are summarized in Table 5.

From these data, Φ_{inj} for TiO_2-**RuPdvb**-*poly*-$[\mathbf{Fe(v\text{-}tpy)_2}]^{2+}$ is significantly lower (≤30%) than Φ_{inj} for TiO_2-**RuP** (100%). Since **RuPdvb** is expected to have a near unity electron injection yield in the polymerized film ($\Phi_{inj(TiO2\text{-}\mathbf{RuPdmb})}$ = 100%), there is a significant decrease in Φ_{inj} for TiO_2-**RuPdvb**-*poly*-$[\mathbf{Fe(v\text{-}tpy)_2}]^{2+}$. It should be noted that the reported net injection yield only accounts for Fe^{III}, and not Ru^{III}, present at 20 ns after the laser flash. Also, photons absorbed by *poly*-$[\mathbf{Fe(v\text{-}tpy)_2}]^{2+}$ at 450 nm are largely lost since the *poly*-$[\mathbf{Fe(v\text{-}tpy)_2}]^{2+}$ chromophore acts as a nonproductive light absorber/filter. An additional contributing factor may arise from the time scale of the injection measurement. Excitation−injection events followed by back electron transfer on the <20 ns time scale are not included in the experimental Φ_{inj} values.

The transient absorption results demonstrate that electropolymerization can be used to incorporate an electron donor as an overlayer on chromophores preattached to a metal oxide surface. The electron donor facilitates directional electron transfer toward the metal oxide surface and slows deleterious back electron transfer. We are currently investigating more elaborate structures with nonabsorbing external donors in the outer layer to prepare chromophore−catalyst assembly structures at the interface for possible DSPEC applications.

CONCLUSIONS

We report here a successful, general strategy for synthesizing and characterizing spatially controlled, multicomponent films on mesoporous TiO_2. The films were prepared by electropolymerization of $[\mathbf{Fe(v\text{-}tpy)_2}]^{2+}$ on both TiO_2 and **RuPdvb**-derivatized mesoporous TiO_2. The Ru:Fe ratio in the overlayer structures can be controlled by the number of reductive electrochemical scan cycles. EDS measurements reveal the films to be inhomogeneous in depth with regard to total concentration and Ru:Fe ratio.

The photostabilities of the TiO_2-**RuPdvb**-*poly*-$[\mathbf{Fe(v\text{-}tpy)_2}]^{2+}$ interfacial structures are enhanced by factors of up to 30 compared to the surface-bound complex alone. Notably, surface stabilization is enhanced relative to an ALD overlayer strategy based on Al_2O_3.

Based on the results of transient absorbance measurements on TiO_2-**RuPdvb**-*poly*-$[\mathbf{Fe(v\text{-}tpy)_2}]^{2+}$, excitation of surface-bound Ru^{II} is followed by electron injection and both fast and slow outside-to-inside $Fe^{II} \rightarrow Ru^{III}$ electron transfer. These results show that the electropolymerized overlayer structure facilitates directional electron transfer toward the metal oxide surface and slows back electron transfer from $TiO_2(e^-)$. The generality of the electropolymerized overlayer approach for synthesis of water stable, multicomponent films is notable and is currently being exploited to prepare interfacial structures for electrocatalysis and DSPEC applications.

ASSOCIATED CONTENT

Supporting Information

Details concerning materials and methods, experimental procedures, eqs S1−S5, EDS analyses, UV/vis absorption spectra, adsorption isotherms, cyclic voltammograms, emission spectra, time-resolved absorption difference spectra, and photostability measurements. This material is available free of charge via the Internet at http://pubs.acs.org.

AUTHOR INFORMATION

Corresponding Authors

*joetemp@unc.edu
*tjmeyer@unc.edu

Author Contributions

†A.M.L. and D.L.A. contributed equally.

Notes

The authors declare no competing financial interest.

ACKNOWLEDGMENTS

K.H. acknowledges support from the UNC EFRC "Center for Solar Fuels", an Energy Frontier Research Center funded by the U.S. Department of Energy, Office of Science, Office of Basic Energy Sciences, under Award No. DE-SC0001011. A.M.L. acknowledges support from the U.S. Department of Energy, Office of Science, Office of Basic Energy Sciences, under Award No. DE-FG02-06ER15788. D.L.A. acknowledges support from a fellowship from the Department of Energy Office of Science Graduate Fellowship Program (DOE SCGF), made possible in part by the American Recovery and Reinvestment Act of 2009, administered by ORISE-ORAU under Contract No. DE-AC05-06OR23100.

REFERENCES

(1) Hagfeldt, A.; Boschloo, G.; Sun, L.; Kloo, L.; Pettersson, H. *Chem. Rev.* **2010**, *110*, 6595.
(2) Song, W.; Chen, Z.; Brennaman, M. K.; Concepcion, J. J.; Patrocinio, A. O. T.; Murakami Iha, N. Y.; Meyer, T. J. *Pure Appl. Chem.* **2011**, *83*, 749.
(3) Youngblood, W. J.; Lee, S.-H. A.; Maeda, K.; Mallouk, T. E. *Acc. Chem. Res.* **2009**, *42*, 1966.
(4) Xu, Y.; Eilers, G.; Borgström, M.; Pan, J.; Abrahamsson, M.; Magnuson, A.; Lomoth, R.; Bergquist, J.; Polívka, T.; Sun, L.; Sundström, V.; Styring, S.; Hammarström, L.; Åkermark, B. *Chem.—Eur. J.* **2005**, *11*, 7305.
(5) Young, K. J.; Martini, L. A.; Milot, R. L.; Snoeberger, R. C., III; Batista, V. S.; Schmuttenmaer, C. A.; Crabtree, R. H.; Brudvig, G. W. *Coord. Chem. Rev.* **2012**, *256*, 2503.
(6) Song, W.; Chen, Z.; Glasson, C. R. K.; Hanson, K.; Luo, H.; Norris, M. R.; Ashford, D. L.; Concepcion, J. J.; Brennaman, M. K.; Meyer, T. J. *ChemPhysChem* **2012**, *13*, 2882.
(7) Eisenberg, R.; Gray, H. B. *Inorg. Chem.* **2008**, *47*, 1697.
(8) Hanson, K.; Brennaman, M. K.; Ito, A.; Luo, H.; Song, W.; Parker, K. A.; Ghosh, R.; Norris, M. R.; Glasson, C. R. K.; Concepcion, J. J.; Lopez, R.; Meyer, T. J. *J. Phys. Chem. C* **2012**, *116*, 14837.
(9) Hanson, K.; Brennaman, M. K.; Luo, H.; Glasson, C. R.; Concepcion, J. J.; Song, W.; Meyer, T. J. *ACS Appl. Mater. Interfaces* **2012**, *4*, 1462.
(10) Moore, G. F.; Blakemore, J. D.; Milot, R. L.; Hull, J. F.; Song, H.-e.; Cai, L.; Schmuttenmaer, C. A.; Crabtree, R. H.; Brudvig, G. W. *Energy Environ. Sci.* **2011**, *4*, 2389.
(11) Gao, Y.; Ding, X.; Liu, J.; Wang, L.; Lu, Z.; Li, L.; Sun, L. *J. Am. Chem. Soc.* **2013**, *135*, 4219.
(12) Concepcion, J. J.; Jurss, J. W.; Hoertz, P. G.; Meyer, T. J. *Angew. Chem., Int. Ed.* **2009**, *48*, 9473.
(13) Ashford, D. L.; Song, W.; Concepcion, J. J.; Glasson, C. R. K.; Brennaman, M. K.; Norris, M. R.; Fang, Z.; Templeton, J. L.; Meyer, T. J. *J. Am. Chem. Soc.* **2012**, *134*, 19189.
(14) Hanson, K.; Torelli, D. A.; Vannucci, A. K.; Brennaman, M. K.; Luo, H.; Alibabaei, L.; Song, W.; Ashford, D. L.; Norris, M. R.; Glasson, C. R. K.; Concepcion, J. J.; Meyer, T. J. *Angew. Chem., Int. Ed.* **2012**, *51*, 12782.
(15) Brown, D. G.; Schauer, P. A.; Borau-Garcia, J.; Fancy, B. R.; Berlinguette, C. P. *J. Am. Chem. Soc.* **2013**, *135*, 1692.
(16) Oyama, N.; Anson, F. C. *J. Am. Chem. Soc.* **1979**, *101*, 3450.
(17) Murray, R. W. *Acc. Chem. Res.* **1980**, *13*, 135.

(18) Cosnier, S.; Deronzier, A.; Moutet, J. C. *J. Electroanal. Chem. Interfacial Electrochem.* **1985**, *193*, 193.
(19) Cosnier, S.; Deronzier, A.; Moutet, J. C. *J. Mol. Catal.* **1988**, *45*, 381.
(20) Abruña, H. D. *Coord. Chem. Rev.* **1988**, *86*, 135.
(21) Aranyos, V.; Hjelm, J.; Hagfeldt, A.; Grennberg, H. *J. Chem. Soc., Dalton Trans.* **2001**, 1319.
(22) Abruña, H. D.; Denisevich, P.; Umaña, M.; Meyer, T. J.; Murray, R. W. *J. Am. Chem. Soc.* **1981**, *103*, 1.
(23) Calvert, J. M.; Schmehl, R. H.; Sullivan, B. P.; Facci, J. S.; Meyer, T. J.; Murray, R. W. *Inorg. Chem.* **1983**, *22*, 2151.
(24) Gould, S.; O'Toole, T. R.; Meyer, T. J. *J. Am. Chem. Soc.* **1990**, *112*, 9490.
(25) Ramos Sende, J. A.; Arana, C. R.; Hernandez, L.; Potts, K. T.; Keshevarz-K, M.; Abruña, H. D. *Inorg. Chem.* **1995**, *34*, 3339.
(26) Moss, J. A.; Yang, J. C.; Stipkala, J. M.; Wen, X.; Bignozzi, C. A.; Meyer, G. J.; Meyer, T. J. *Inorg. Chem.* **2004**, *43*, 1784.
(27) Cecchet, F.; Alebbi, M.; Bignozzi, C. A.; Paolucci, F. *Inorg. Chim. Acta* **2006**, *359*, 3871.
(28) Nie, H.-J.; Shao, J.-Y.; Wu, J.; Yao, J.; Zhong, Y.-W. *Organometallics* **2012**, *31*, 6952.
(29) Zhong, Y.-W.; Yao, C.-J.; Nie, H.-J. *Coord. Chem. Rev.* **2013**, *257*, 1357.
(30) Li, M.; Zhang, J.; Nie, H.-J.; Liao, M.; Sang, L.; Qiao, W.; Wang, Z. Y.; Ma, Y.; Zhong, Y.-W.; Ariga, K. *Chem. Commun.* **2013**, *49*, 6879.
(31) Norris, M. R.; Concepcion, J. J.; Glasson, C. R. K.; Fang, Z.; Lapides, A. M.; Ashford, D. L.; Templeton, J. L.; Meyer, T. J. Submitted.
(32) Langmuir, I. *J. Am. Chem. Soc.* **1918**, *40*, 1361.
(33) Marcus, R. A. *J. Phys. Chem.* **1989**, *93*, 3078.
(34) Ito, A.; Stewart, D. J.; Knight, T. E.; Fang, Z.; Brennaman, M. K.; Meyer, T. J. *J. Phys. Chem. B* **2013**, *117*, 3428.
(35) Katoh, R.; Furube, A.; Yoshihara, T.; Hara, K.; Fujihashi, G.; Takano, S.; Murata, S.; Arakawa, H.; Tachiya, M. *J. Phys. Chem. B* **2004**, *108*, 4818.
(36) Potts, K. T.; Usifer, D. A.; Guadalupe, A.; Abruña, H. D. *J. Am. Chem. Soc.* **1987**, *109*, 3961.
(37) Trammell, S. A.; Meyer, T. J. *J. Phys. Chem. B* **1998**, *103*, 104.
(38) O'Regan, B.; Li, X.; Ghaddar, T. *Energy Environ. Sci.* **2012**, *5*, 7203.
(39) Park, S.-H.; Lim, J.; Song, I. Y.; Atmakuri, N.; Song, S.; Kwon, Y. S.; Choi, J. M.; Park, T. *Adv. Energy Mater.* **2012**, *2*, 219.
(40) Song, W.; Luo, H.; Hanson, K.; Concepcion, J. J.; Brennaman, M. K.; Meyer, T. J. *Energy Environ. Sci.* **2013**, *6*, 1240.
(41) Hanson, K.; Losego, M. D.; Kalanyan, B.; Ashford, D. L.; Parsons, G. N.; Meyer, T. J. *Chem. Mater.* **2013**, *25*, 3.
(42) Juban, E. A.; Smeigh, A. L.; Monat, J. E.; McCusker, J. K. *Coord. Chem. Rev.* **2006**, *250*, 1783.
(43) Durrant, J. R.; Haque, S. A.; Palomares, E. *Coord. Chem. Rev.* **2004**, *248*, 1247.
(44) Piotrowiak, P.; Galoppini, E.; Wei, Q.; Meyer, G. J.; Wiewiór, P. *J. Am. Chem. Soc.* **2003**, *125*, 5278.
(45) Bergeron, B. V.; Kelly, C. A.; Meyer, G. J. *Langmuir* **2003**, *19*, 8389.